frontiers | Frontiers in Environmental Science

TYPE Original Research
PUBLISHED 25 November 2022
DOI 10.3389/fenvs.2022.1085326

OPEN ACCESS

EDITED BY
Tingting Liu,
Xi'an Polytechnic University, China

REVIEWED BY
Nabeel Khan Niazi,
University of Agriculture Faisalabad, Pakistan
Gao Lizhen,
Shanxi University, China

*CORRESPONDENCE
Haitao Wang,
wanghaitao@tiangong.edu.cn
Na Chang,
changna@tiangong.edu.cn

SPECIALTY SECTION
This article was submitted to Toxicology, Pollution and the Environment, a section of the journal Frontiers in Environmental Science

RECEIVED 31 October 2022
ACCEPTED 14 November 2022
PUBLISHED 25 November 2022

CITATION
Hussain Z, Zhang H, Chang N and Wang H (2022), Synthesis of porous materials by the modification of coal fly ash and its environmentally friendly use for the removal of heavy metals from wastewater.
Front. Environ. Sci. 10:1085326.
doi: 10.3389/fenvs.2022.1085326

Synthesis of porous materials by the modification of coal fly ash and its environmentally friendly use for the removal of heavy metals from wastewater

Zawar Hussain[1], Hao Zhang[2], Na Chang[2]* and Haitao Wang[1]*

[1]School of Material Science and Engineering, Tiangong University, Tianjin, China, [2]School of Textile Science and Engineering, Tiangong University, Tianjin, China

Wastewater is a complex mixture of many pollutants, where the high-risk pollutants are heavy metals (HMs) in industrial wastewater due to their difficult removal. In this study, the waste CFA was used as the main raw material for production of new innovated flocculants porous particles by modification of coal fly ash (CFA) using a multi-step base–acid–base (NaOH–HCl–NaOH) modification method. The morphological structure and elemental composition of the prepared MCFA were analyzed through characterization analysis, i.e., SEM, EDX, FT-IR, BET, XPS, and XRD. Results found that the surface area of the flocculant particles of MCFA was increased from 5.241 to 32.011 m^2/g, which increased the adsorption process of HMs (Mn^{2+}, Cu^{2+}, Ni^{2+}, and Pb^{2+}). The maximum removal efficiencies (Re %) of MCFA for Mn^{2+}, Cu^{2+}, Ni^{2+}, and Pb^{2+} were recorded at 94.26%, 95.88%, 71.04%, and 99.91%, respectively. The Freundlich isotherm model was fitted for the adsorption process, and the maximum adsorption amounts of MCFA for Mn^{2+}, Cu^{2+}, Ni^{2+}, and Pb^{2+} were 558.9219, 0.4341, 210.9737, and 12.1957 mg/g, respectively. Moreover, the kinetic model indicated that physicochemical adsorption occurred between the adsorbate materials and the adsorbent.

KEYWORDS

porous materials, coal fly ash, acid–base modification, wastewater, adsorption

1 Introduction

Water pollution due to anthropogenic activities such as industrial operations is the most concerning issue in the modern world. Industries, which are the backbone of the national economy and also a major source of water pollution as they discharge high-strength chemical wastewater, mainly comprise organic and inorganic pollutants, thus polluting groundwater and soil and ultimately posing serious health problems (Younas et al., 2021; Ayaz et al., 2019). Industrial wastewater is a complex mixture of pollutants, mostly consisting of high concentration of heavy metals (HMs) (Gan et al., 2020; Wu

et al., 2016). The main sources are mining operations, tanneries, and electronics for Cu (Han et al., 2016); batteries, fertilizers, electroplating, tanneries, mining, and metal processing for manganese (Mn) (Peligro et al., 2016); paint industries, plastics, mining, textile industries, and preservative producing industries for Pb (Ge & Choi, 2017); and tanning and dye manufacturing for plastics, paints, and textile industries for chromium (Cr) (Peydayesh et al., 2019). The discharge of HM-contaminated wastewater is not only polluting groundwater and soil but is also entering the human body from contaminated crop plants grown in contaminated soil and/or irrigated with contaminated water (Clemens and Ma, 2016). The removal and management of such high-risk pollutants from wastewater is very difficult due to their persistence and toxicity in the environment (Wu et al., 2016).

There are many methods for wastewater treatment and removal of pollutants, but adsorption is the most efficient and simple method for treatment of wastewater and removal of toxic HMs from industrial wastewater (Chen et al., 2015; Hong et al., 2019). Various materials are used as adsorbents, such as activated carbon (Gan et al., 2020; Lee et al., 2017), chitosan (Zhu et al., 2019), zeolite (Cheng et al., 2018), bentonite (Niu et al., 2020), agriculture residues (Lee et al., 2017), hydrogel beads (Zhang et al., 2022), and clay materials (Athman et al., 2020), and have gathered much attraction and are in use from many years for wastewater treatment. Recently, waste coal fly ash has been reported as a recycled material that can be reused for removal of pollutants, but it needs modification to enhance the adsorption efficiency (Hussain et al., 2022), whereas adsorption is considered a cheaper and very simple method (Song et al., 2018; Maleki et al., 2019).

In the past few years, much research has been conducted on the modification and its environmentally friendly use of CFA for adsorption. Nguyen et al. (2020) conducted a study on the modification of CFA by NaOH and its use in the removal of Cd $^{2+}$ and Hg^{2+}. The pore size of modified fly ash has been increased by 50 nm. The study stated that the removal percentage of Cd^{2+} has been increased from 65% to 97% by the treatment of coal fly ash. Bai et al. (2019) studied zeolite, prepared by the mixture of two different ashes (CFA and solid fuel residue ash), for removal of HMs. BET analysis indicated that the surface area of synthetic zeolite from fly ash has increased by 288.55 m^2/g. The results were calculated by kinetic and isotherm models, and the results were in the $Pb^{2+} > Cr^{3+} > Cu^{2+} > Cd^{2+} > Zn^{2+}$ order. Salehin et al. (2016) studied the modification of activated carbon by oil fly ash by passing CO_2 and used as an HM adsorbent, the surface area of modified/synthetic activated carbon was increased by 2.5 times. The results indicated that the removal efficiency % of Cu and Pb was 99% and 99.3%, respectively, at pH 5. Maria Visa and Anca Duta studied the substrate synthesized from fly ash using TiO_2 as a semiconductor by hydrothermal processing. The synthetic substrate was used for removal of HMs (Cd^{2+} and Cu^{2+}) and surfactants from synthetic wastewater (Visa and Chelaru, 2014). Wang et al. (2021). studied fly ash from two different coal power plants and modified it with NaOH for the removal of Pb (II) from wastewater. The study found that the surface area was increased by 30.37 and 49.46 m^2/g after modification of the CFA of both coal power plants, respectively. The results indicated that more than 146 and 165 mg/g of Pb (II) was adsorbed by both fly ashes, respectively. All previous studies indicated that there is a big loophole that is not covered by the past investigations, the simple modification of coal fly ash has occurred, but no new materials were prepared. The current study identified and filled the research gap by the invention of new flocculant porous particles by the modification of the multi-step base–acid–base method.

This research aims to decrease the waste of coal fly ash and utilize it for treatment of wastewater. However, many studies have been reported on the modification of coal fly ash and its use as a heavy metal adsorbent, but more simple and advanced modification is needed to modify the coal fly ash and adsorption of HMs. In this research, the porous materials of coal fly ash were prepared by the physico-chemical method of multi-step acid–base modification. By this modification of coal fly ash, the porous adsorbent with completely different physical and chemical properties was separated from the floating layer of the reaction suspension. The MCFA has increased surface area by six times than that of waste coal fly ash and improved hydrophilicity due to the increase in the number of oxygen-containing groups (OCG). The increase in OCG also improved the chelating ability of HMs. It also has lightweight and increased suspending properties in aqueous solutions, which can reduce the sedimentation rate of MCFA and thus extend its contact time with the adsorbates. In this work, the MCFA is used for removal of four HMs (Mn^{2+}, Cu^{2+}, Ni^{2+}, and Pb^{2+}) from wastewater that have a higher adsorption capacity.

2 Materials and methods

2.1 Chemical material

Waste coal fly ash was taken from the coal power plant located in Yulin city, Shanxi Province of China. Chemical reagents were purchased from Tianjin Chemicals, China. HM ion salts like sulfate and nitrate and chlorine salts of Mn^{2+}, Cu^{2+}, Ni^{2+}, and Pb^{2+} were purchased from the Chemistry and Chemical Institute of Tiangong Laboratory, Tianjin, China.

2.2 Formation of mesoporous materials of coal fly ash

CFA (40 g) was placed in a 2,000-ml flask containing 800 ml of NaOH (5%) solution and stirred with a magnetic stirrer at

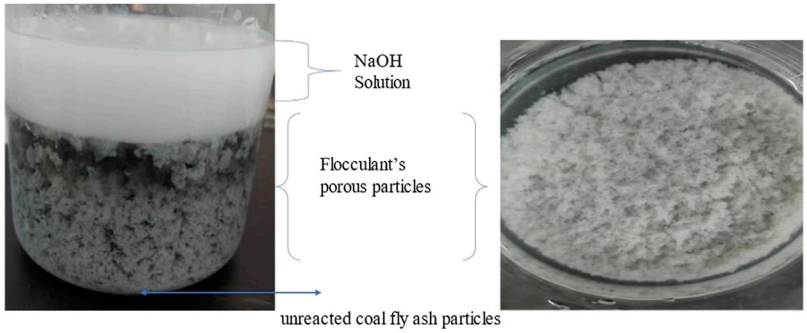

FIGURE 1
Flocculant's porous particles of MCFA by the treatment of the multi-step base–acid–base (NaOH-HCl-NaOH) method.

40°C for 4 h. The solution was then cooled down to room temperature, and 80 ml HCl (10%) was added into the alkali–CFA solution. The solution was then ultrasonicated for 5 h at 40°C into an ultrasonic cleaner (KH-250E). Then, 800 ml water was mixed with a CFA–acid solution. Then, the NaOH (10%) solution was added dropwise until the CFA particles flocculated. In the reaction of the suspension, the original coal fly ash was disintegrated and transformed into cotton-like flocculating particles. Some unreacted coal fly ash particles were also present on the bottom of the solution, but only these flocculating particles were separated from the unreacted coal fly ash (Figure 1) by gravity flotation and then filtered. After neutralizing with distilled water, the filtered modified flocculant porous particles of CFA (MCFA) were dried in a furnace (YLD-2000) for 8 h at 250°C. The flocculant's porous particles of the MCFA adsorbent were ready for HM adsorption.

2.3 Adsorption experiments

The sorption process of selected HMs (Mn^{2+}, Cu^{2+}, Ni^{2+}, and Pb^{2+}) was carried out in a batch shaker machine at 30°C, and the concentration of HMs before and after adsorption of HMs was determined by an Abs meter (TAS-990 Super). The effect of different dosages (0.2, 0.4, 0.6, 0.8, and 1.0 g) of the MCFA adsorbent was analyzed in 400 ml solution of Mn^{2+}, Cu^{2+}, Ni^{2+}, and Pb^{2+} with 100 mg/L concentrations of each metal for 1 h. The effects of different HM anions (Cl^{-}, SO^{2-}_{4}, and NO^{-}_{3}) were observed for MCFA at the same HM concentration (100 mg/L) of each ion and adsorbent dosage (1.0 g) for the removal of 400 ml of solution for 1 h.

2.4 Characterization of modified flocculant particles of coal fly ash

The surface morphology and elemental composition of unmodified CFA, modified flocculant particles (MCFA), and MCFA (1.0 g dosage) after adsorption of HMs (MCFA-HMs) were analyzed by EDX and SEM (Gemini-500) for a mixed four-HM (Mn^{2+}, Cu^{2+}, Ni^{2+}, and Pb^{2+}) sample with 100 mg/L concentration of each metal. The BET (Autosorb iQ Station 1) analysis was used for determination of the surface area and pore size. XPS analysis was analyzed by spectroscopy of MCFA and after loaded HM (MCFA-H.M) samples, and the same dosage and sample of the adsorbed heavy metals were used as EDX and SEM to analyze the XPS. The morphological structure and elemental peaks were investigated by XRD on the prepared mesoporous material loaded with HMs (Mn^{2+}, Cu^{2+}, Ni^{2+}, and Pb^{2+}).

2.5 Calculations and measurements analysis

Removal efficiency (R %) and adsorption capacity (Q) of all the samples in Abs were calculated using following equations (Yuan et al., 2021).

$$\text{Adsorption Qe} = \frac{(Co - C1)*\text{V},}{m} \quad (1)$$

$$\text{R \%} = \frac{(Co - C1)}{Co}*100 \quad (2)$$

where C0 is the original concentration of the HM solution, C1 is the after adsorption concentration of the HMs, m is the weight of the mesoporous material, and V is the volume.

where C1 was measured by the following formula,

$$\frac{C1}{C0} = \frac{Abs1\,(after\,adsorption)}{Abs0\,(before\,adsorption.)} \quad (3)$$

2.6 Adsorption models

The adsorption isotherm models (Langmuir and Freundlich) of different HM concentrations (20, 40, 60, 80, and 100 mg/L)

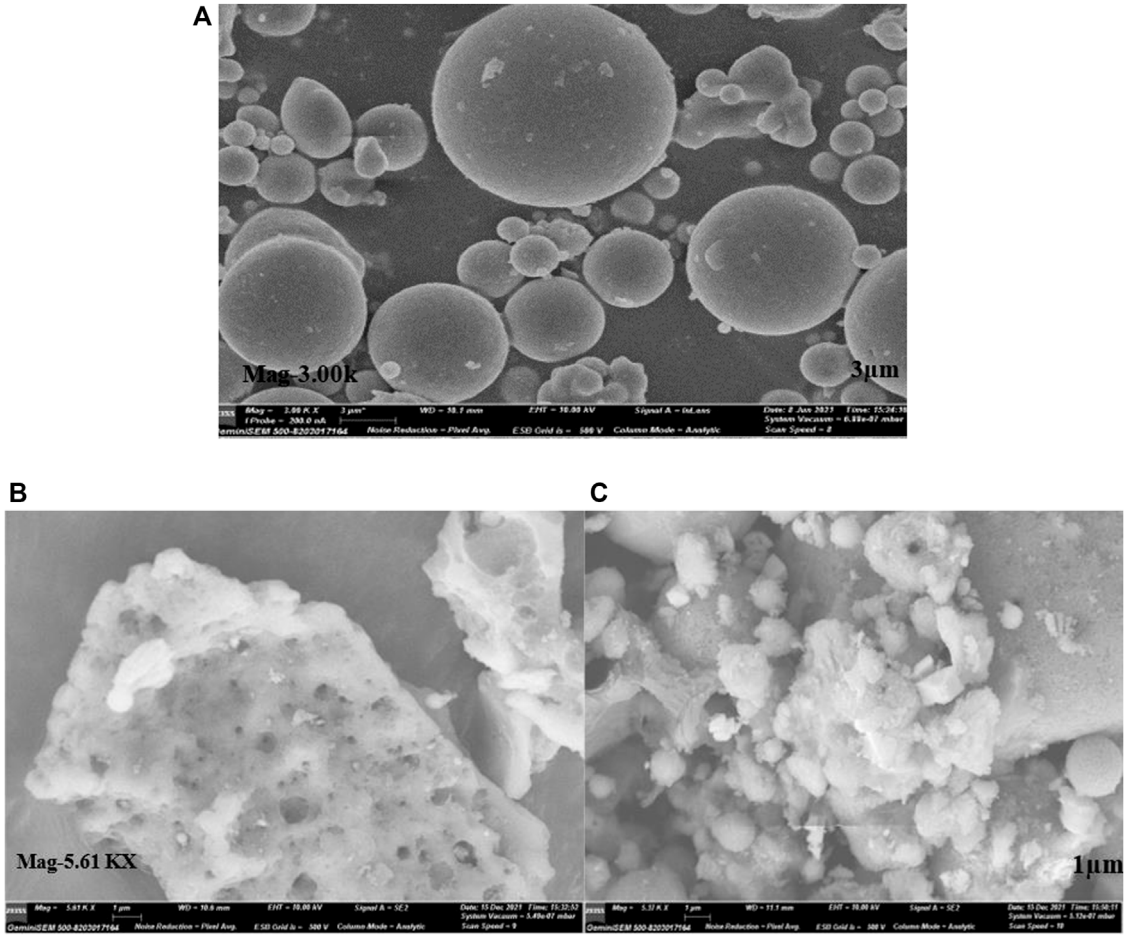

FIGURE 2
SEM images of UMCFA, **(A)** MCFA, **(B)** MCFA-HM, and **(C)**.

were analyzed individually in 200 ml of simulated water using a lower dosage of the adsorbent (0.2 g) by each HM for 1 h. The adsorption kinetics was also determined at different times (5, 10, 15, 20, 25, 30, 40, 50, and 60 min) at the same adsorbent dosage (0.2 g) with each metal concentration (100 mg/L).

Isotherm models were calculated by the following methods,

$$\text{Freundlich isothermal: } q_e = K_F + \frac{1}{n}C_e \quad (4)$$

$$\text{Langmuir isothermal: } \frac{qe}{Ce} = K_L qmax - K_L q_e \quad (5)$$

where Qe: adsorption (mg g^{-1}); Ce: concentration of metal salts (mg L^{-1}); K_L: coefficient adsorption; K_f: coefficient of the Freundlich model.

Kinetic model calculations,

$$2^{nd}\ \text{pseudo} - \text{order}: \frac{t}{q} = \frac{t}{qe} + \frac{1}{k_2 q_e^2} \quad (6)$$

$$1\text{st pseudo} - \text{order: } (Q_e - Q) = \ln Q_e - k1t \quad (7)$$

where T: time in minutes; Q: adsorption (mg g^{-1}); Qe: adsorption capacity; and $K_{2\ \text{and}\ 1}$: rate constant of second pseudo-order and first pseudo-order

3 Results and discussions

3.1 Characterization analysis

3.1.1 SEM analysis

Figure 2 shows the morphological characterization of UMCFA, MCFA, and MCFA-HM. SEM results indicated that the modification by the NaOH–HCl–NaOH method deformed the crystalline spherical ball structure of UMCFA (Figure 2A) into porous structure (i.e., wool like structure) of flocculant less weight particles of MCFA so that these particles

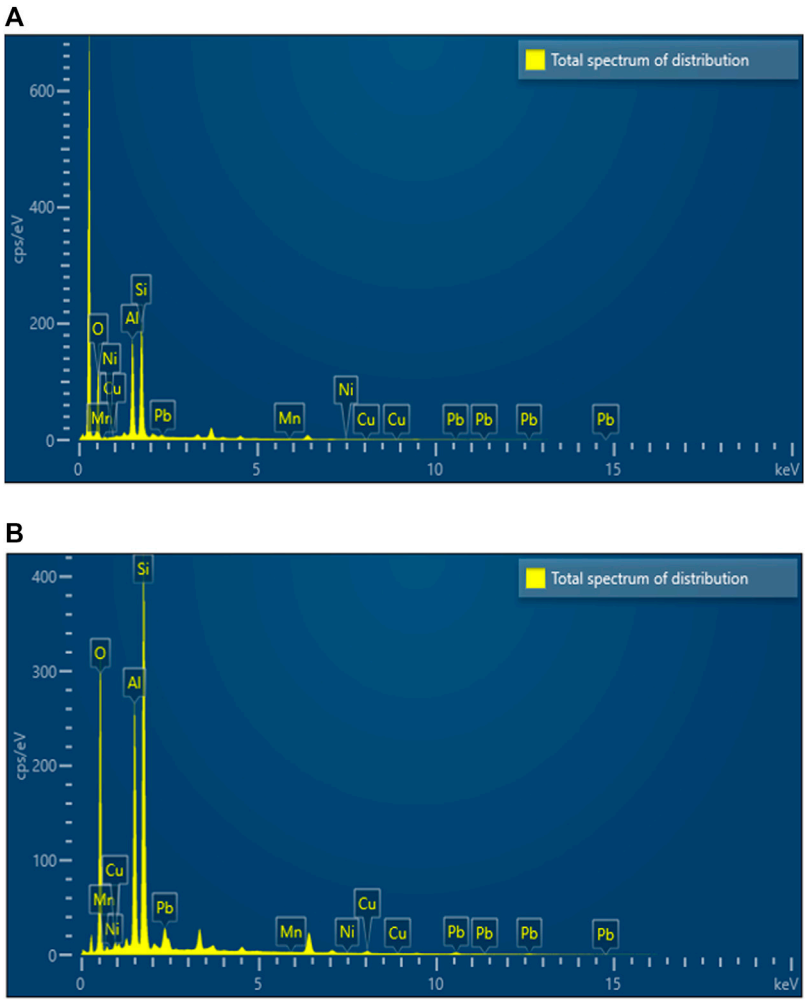

FIGURE 3
EDX spectrum composition of MCFA **(A)** and MCFA-HM **(B)**.

were flocculated in the solution (Figure 2B), and in Figure 2C, some loaded attachments can be clearly observed, which indicated that HMs (Mn^{2+}, Cu^{2+}, Ni^{2+}, and Pb^{2+}) were loaded on the surface of MCFA after adsorption. The small spherical ball like structure of UMCFA particles had different sizes of holes with various thickness and densities (Gao et al., 2015; Shah et al., 2013), which refer to the physical and chemical effects during the alkali–acid–alkali reaction and ultrasonic treatment with CFA that transformed the spherical hollow balls into wool-like flocculant particles (Figure 2B), so the dense structure turned into an amorphous structure. This rough amorphous structure of MCFA could enhance the active sites of CFA particles, and the porous structure resulted in increased adsorption of HMs (Wang et al., 2021).

3.1.2 EDX analysis

An EDX test was carried out to check the variation of surface element distribution on the surface of MCFA before and after adsorption. Figure 3 and Table 1 show the EDX composition results of MCFA and MCFA-HM, respectively. Results indicated that the peaks of different element compositions are different before and after adsorption of HMs. The difference of MCFA composition could affect the adsorption capacity (Mushtaq et al., 2020). After adsorption of HMs, the new peaks of Mn^{2+}, Cu^{2+}, Ni^{2+}, and Pb^{2+} metal ions appeared, with the peaks of Pb^{2+} and Cu^{2+} increasing significantly than those of Mn^{2+} and Ni^{2+}. The peaks of the main components of CFA (i.e., O, Al, and Si) have a big difference before and after adsorption. The peak intensity of O has a significant decrease in MCFA-HM. It can be due to the MCFA, which mainly combines the HM ions with the oxygen-

TABLE 1 Elemental composition of MCFA and MCFA-HM.

Elements	MCFA			MCFA-HM		
	Weight %	Weight % sigma	Apparent concentration	Weight %	Weight % sigma	Apparent concentration
O	43.97	0.09	24.98	47.90	0.06	58.73
Al	22.04	0.05	13.17	15.53	0.03	18.00
Si	33.30	0.07	15.64	28.03	0.04	29.37
Mn	0.03	0.03	0.01	0.05	0.02	0.05
Ni	0.05	0.04	0.03	0.07	0.02	0.07
Cu	0.00	0.04	0.00	2.38	0.03	2.39
Pb	0.60	0.09	0.42	6.05	0.06	5.17

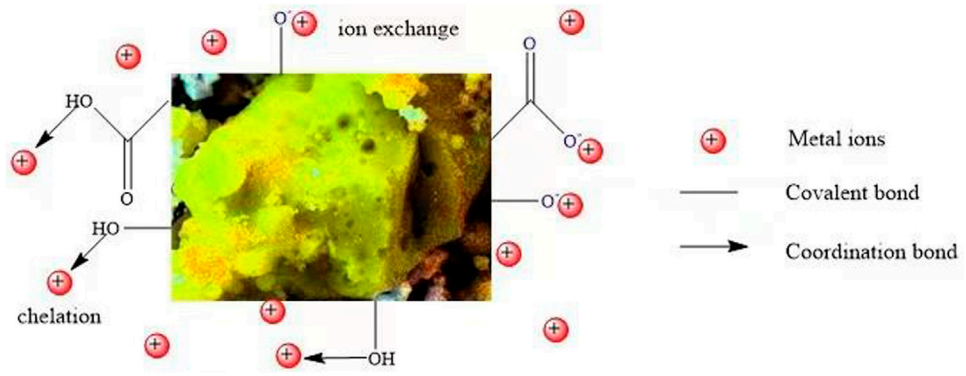

FIGURE 4
Adsorption mechanism of HM ions on the surface of MCFA.

containing groups on its surface. So, after adsorption, a significant number of the surface oxygen-containing groups have been covered by the HM ions, and the surface oxygen content has experienced a significant decline.

Figure 4 shows the electrostatic interaction and bonding mechanism of MCFA and metal ions to the surface of MCFA active sites. In this study, it was regarded to two main binding forces between the metal ions and MCFA: A. the electrostatic attraction among positively charged diatomic metal ions and negatively charged dissociate surface oxygen-containing groups (hydroxyl anions $-O^-$ and carboxyl anions $-COO^-$); B. the sequestration bonding among the hybridized metal ions and oxygen atom with coordinate lone pair electrons. The previous study stated that because of the active site of MCFA, the Pb^{2+} was adsorbed successfully due to the ion exchange of HMs to the adsorbent (Iqbal et al., 2009). The multiple binding forces led to a complicated adsorption behavior of HM ions on the MCFA surface.

3.1.3 BET analysis

The BET results are shown in Figure 5 and Table 2. The BET curve shows the adsorption behavior of N_2 molecules on the surface of MCFA and UMCFA and had a high correlation coefficient to the II type isothermal adsorption model (more than 0.999). The MCFA had a typical inverse S-shape adsorption isothermal curve, which indicated the adsorption of N_2 molecules on the MCFA surface in a complex behavior. With the increase of N_2 partial pressure, the adsorption showed a trend of transforming from monolayer adsorption to multimolecular layer adsorption. This was relatively due to the adsorption behavior of non-polar molecules on the inorganic adsorbent surface. The complicated adsorption behavior indicated by the combination of MCFA and the adsorbate is driven by both physical and chemical factors.

Table 2 shows the surface area comparative results of UMCFA and MCFA. The results stated that the surface area of the prepared porous particles has increased from 5.241 to

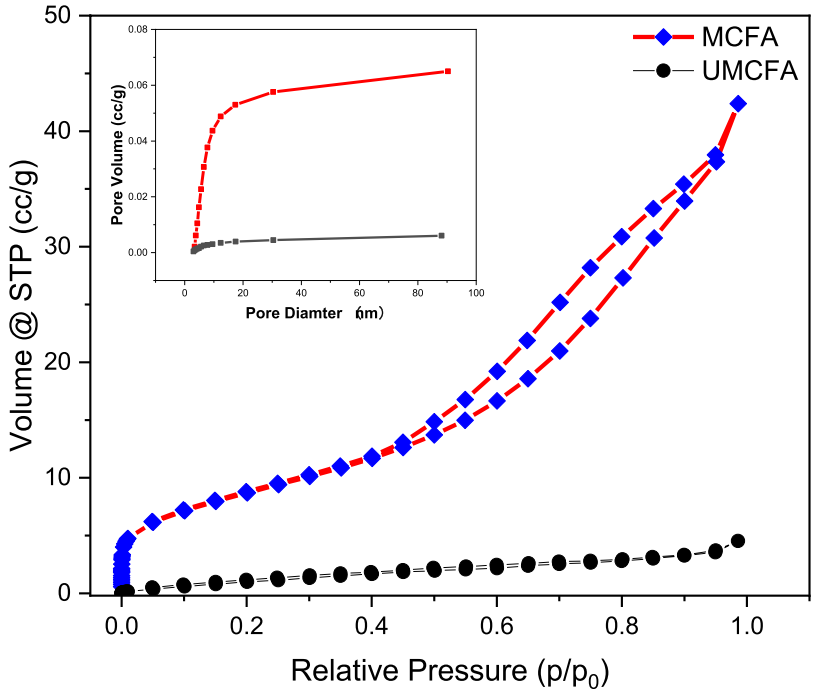

FIGURE 5
BET analysis of MCFA and UMCFA.

TABLE 2 BET comparison analysis of before and after modification of CFA.

	Slope (1/g)	Intercept (1/g)	Correlation coefficient (R)	Constant (C)	Surface area (m^2/g)
UMCFA	574.326	9.016e+01	0.999	7.370	5.241
MCFA	107.163	1.630e+001	0.999	66.753	32.011

32.011 m^2/g. The modification of CFA by NaOH–HCl–NaOH has increased the surface area by six times. It is concluded that the large surface area of the adsorbent increased the adsorption process because the reaction of basic and acidic solutions with CFA increased the active site (Anuar, 2020). The surface area was increased due to the transformation of dense spherical structure to an amorphous wool-like structure under the combined physiochemical effects.

3.1.4 FT-IR spectrum analysis of UMCFA and modified flocculant particles of coal fly ash

The infrared spectra of UMCFA and MCFA are shown in Figure 6. The results indicated that the MCFA peaks were differentiated than those of UMCFA. The width of the MCFA peak has increased at 3,438 cm^{-1}, which indicates that O-H groups are formed on the surface of MCFA after modification by the alkali–acid–alkali reaction. The stretching vibration of the O-H group on the surface of MCFA was due to NaOH modification of CFA (Shah et al., 2013). In addition, the symmetrical peaks of carboxylic, -COO^-, and C-O^- were established at 1,625, 1,408, and 1,082 cm^{-1}, respectively, on the surface of MCFA.

The FT-IR results showed that after alkali–acid–alkali reactions, oxygen-containing groups, including carboxylic and hydroxyl groups (-OH and -COOH), had formed in abundance on the surface of MCFA, and this was considered the key factor for the increase in adsorption capacity of HMs. First, the dissociated carboxyl and hydroxyl anions had strong electrostatic attractions to divalent metal cations; Second, the plentiful oxygen atoms in the undissociated carboxyl and hydroxyl groups can also combine the metal cations *via* chelation bonding. The FT-IR analysis found the complex

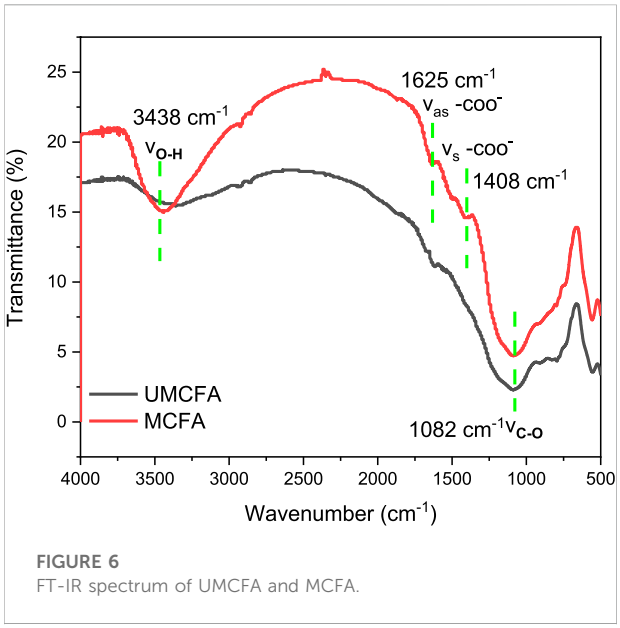

FIGURE 6
FT-IR spectrum of UMCFA and MCFA.

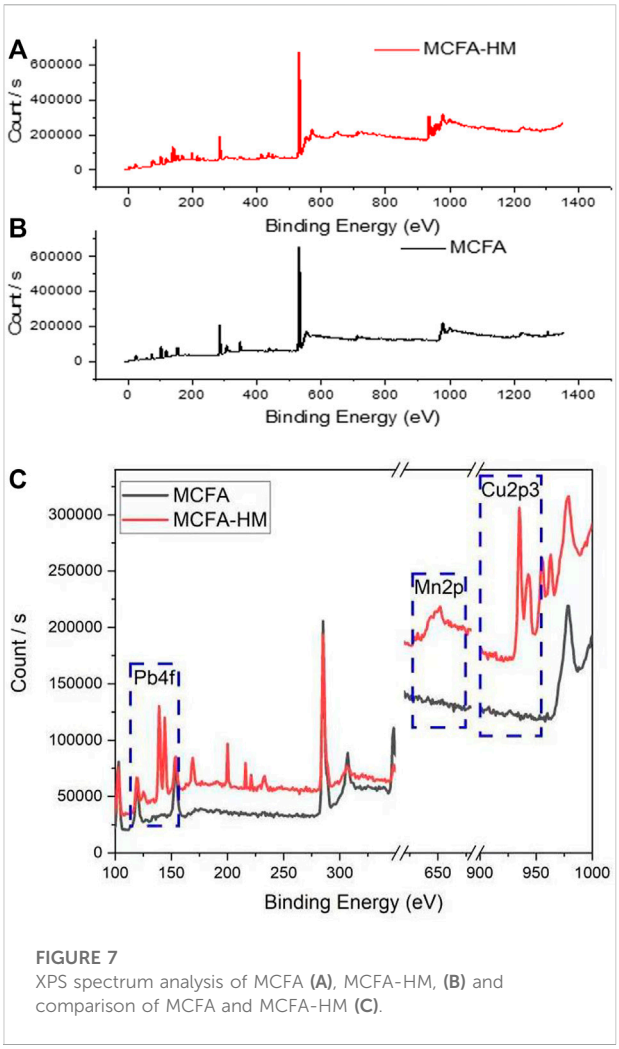

FIGURE 7
XPS spectrum analysis of MCFA **(A)**, MCFA-HM, **(B)** and comparison of MCFA and MCFA-HM **(C)**.

binding forces between the MCFA and the adsorbate, which was in accordance with the analysis of the adsorption mechanism.

3.1.5 XPS analysis

Figure 7A shows the peaks of the main components (Al2p, Si2p, C1s, and O1s) of MCFA, but after the adsorption of HMs, new peaks were observed on the surface of MCFA. The new peaks of Pb 4f, Mn 2p, and Cu 2p3 could be clearly observed in Figures 7B,C.

Figure 7C shows the clear difference between MCFA and MCFA-HM. The new peaks appeared at around 140, 200, 230, 430, 450, 650, and 940 eV of Pb4f, Mn2p, and Cu2p3 on the MCFA adsorbent. The peak intensity of Mn2p was found to be weaker than that of Pb4f and Cu2p3, and Ni2p3 did not appear. This phenomenon could be explained by competitive adsorption behavior among different metal ions in a mixed system. The electron cloud density of O1s atoms decreased as the binding energy value of the adsorbed HM peaks became higher, which was due to the availability of functional groups on the surface of MCFA and HM ions (Wang et al., 2021).

The Pb^{2+} and Cu^{2+} have stronger combinations with MCFA, which could be due to the following factors: A. Pb^{2+} had smaller hydrated ionic radius, so its ion exchange capacity to the dissociated hydroxyl and the carboxyl groups was higher, and the free electrons in the oxygen atom could make chemical bonding by ion exchange between the oxygen atom and metals (Lavall et al., 2007); B. Cu^{2+} had a more stabilized chelating ring structure with the oxygen-containing groups on the MCFA surface. Generally, the complex adsorption behaviors led to an adsorptive selectivity of MCFA for different metal ions, which indicated the possibility of using MCFA for recycling of some unique constituents from the HM-contaminated wastewater.

3.1.6 XRD pattern analysis

Figure 8 shows the X-ray diffraction patterns of UMCFA and MCFA before and after adsorption of HMs. The XRD of UMCFA observed many peaks, and the structure was crystalline, but after the modification of CFA, no more peaks were observed after the modification of CFA and the structure became amorphous, which was due to the destruction of the crystalline (quartz and mullite) texture under the physical and chemical effects (Qiu et al., 2018). However, many peaks appeared after the adsorption of HMs at different degrees like 16.5°, 26.6°, 27.8°, 29°, and 29.9°, which was due to the deposition of heavy metallic salts on the MCFA surface to build sediments with new crystallographic forms. The results proved that HM ions were loaded successfully on the surface of the MCFA.

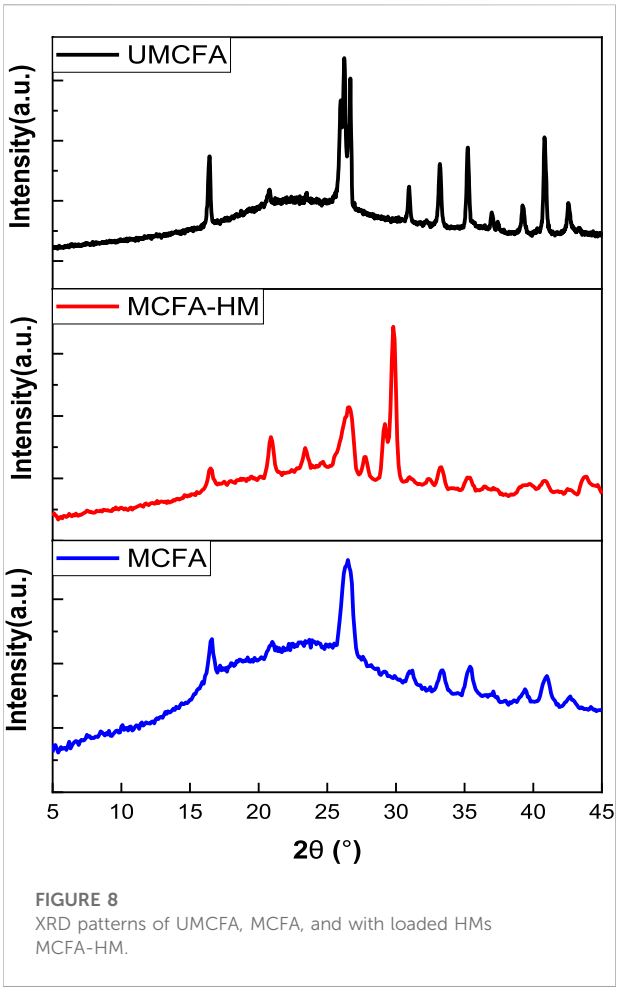

FIGURE 8
XRD patterns of UMCFA, MCFA, and with loaded HMs MCFA-HM.

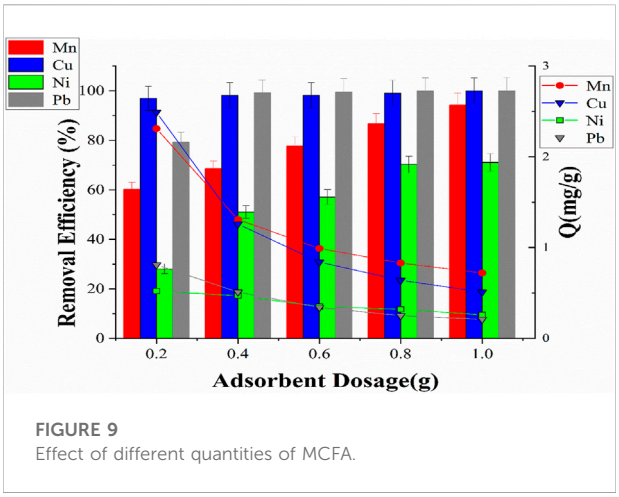

FIGURE 9
Effect of different quantities of MCFA.

3.2 Sorption experiments

3.2.1 Effect of different dosage of modified flocculant particles of coal fly ash

The maximum adsorption capacity and removal efficiency (%) of HMs (Mn^{2+}, Cu^{2+}, Ni^{2+}, and Pb^{2+}) at different dosages of MCFA are shown in Figure 9. The adsorbent dosage is a key factor for the adsorption of HMs (Niu et al., 2020) since a higher dosage provides more adsorption sites that could increase the removal efficiency, but as the dosage increases, the adsorption capacity decreases due to the decreased utilization ratio of the adsorbent. The removal efficiency of HMs was increased as the amount of the MCFA adsorbent was increased. The maximum removal efficiency was recorded as 89.27% and 76.94% for Pb^{2+} and Cu^{2+}, respectively, at a lower dosage of 0.2 g of the MCFA adsorbent. As the dosage amount was increased to 1.0 g, the removal efficiency reached 99.91% and 95.88% of Pb^{2+} and Cu^{2+}, respectively. This might be a higher adsorbent dosage that provides maximum active sites to HMs, thus resulting in maximum removal of HM concentration by the adsorbent (Yang et al., 2010). The previous study also indicated that the removal efficiency of Pb^{2+} ion was higher than that of other HMs (Tang et al., 2019) because the Pb^{2+} ion overloaded faster on the active sites of the adsorbent (Niu et al., 2020).

A similar trend for the adsorption capacity of Mn^{2+} and Ni^{2+} was also observed. The removal efficiency is *vice versa* to the adsorption capacity in this adsorption process. The results indicated that the adsorption capacity (Q mg/g) decreased from a lower dosage to a higher dosage of MCFA. The maximum adsorption capacity was recorded at 2.52 and 2.31 mg/g for Ni^{2+} and Mn^{2+}, respectively, at a lower dosage (0.2 g) of MCFA. For industrial wastewater treatment, a higher dosage of the adsorbent can increase the operating cost and the amount of solid waste. In this study, the removal efficiencies for HMs can be attained at a relatively lower dosage of MCFA. This result proves that MCFA has a great advantage in the application for the removal of HMs from wastewater.

3.2.2 Adsorption isotherm models

Langmuir and Freundlich models are the two isotherm parameters that are used to describe the relationship between adsorbate concentrations and adsorbents (Juang et al., 2006). Adsorption isotherm models discriminate the maximum adsorption capacity of adsorbed pollutants and describe the adsorption properties, i.e., monolayer adsorption or multilayer adsorption or both (Ayari et al., 2008). Figure 10 and Table 3 show the adsorption mechanisms of Mn^{2+}, Cu^{2+}, Ni^{2+}, and Pb^{2+} ions by the MCFA adsorbent. Isotherm parameters showed that the fitting degree to Freundlich models was $R^2 > 0.99$, which indicated the driving forces of the adsorption behaviors were determined by both physical and chemical interactions, and the complex adsorption mechanisms resulted in a combination of monolayer and multilayer adsorption. Results demonstrated that the adsorption process may be monolayer adsorption on the surface of the adsorbent (He et al., 2018).

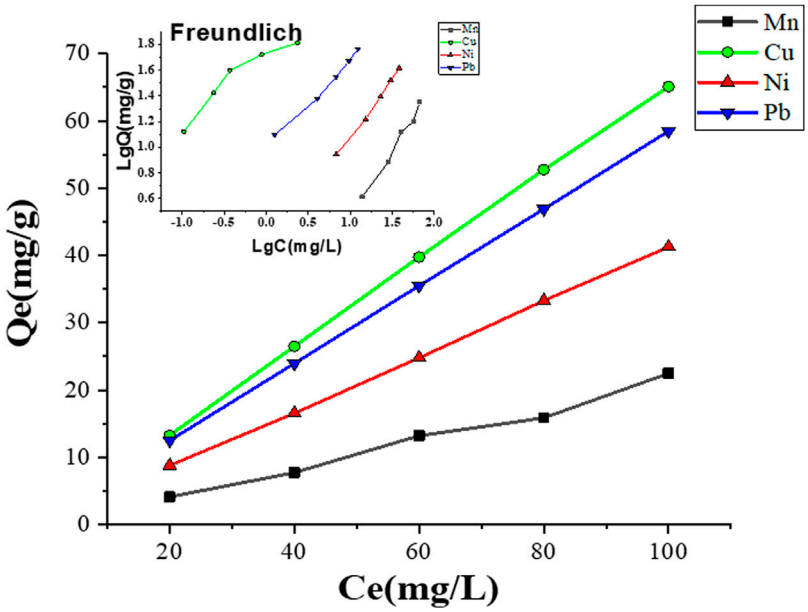

FIGURE 10
Isotherm curves for MCFA adsorption of HMs.

TABLE 3 Langmuir and Freundlich isotherm parameters of adsorption of four HMs by MCFA.

Model	Parameter	Mn^{2+}	Cu^{2+}	Ni^{2+}	Pb^{2+}
Langmuir	K_L (L/g)	0.0064	0.0129	0.0038	0.0092
	Q_m (mg/g)	558.9219	0.4341	210.9737	12.1957
	R2	0.1858	0.9961	0.5296	0.8247
Freundlich	K_F (mg/g) (L/mg)1/n)	4.0523	51.0858	1.5024	10.1883
	nf	0.9459	2.0052	1.1066	1.4890
	R2	0.9824	0.9025	0.9961	0.9905

Table 3 shows the different parameters of the isotherm model. Results indicated that the values of the correlation coefficient (R^2) for Mn^{2+}, Ni^{2+}, and Pb^{2+} were higher (R^2 > 0.98) by the Freundlich model, but the value of the correlation coefficient (R^2) for Cu^{2+} was higher (R^2 > 0.99) by the Langmuir model, which indicated that the adsorption mechanism of Cu^{2+} on the surface of MCFA was different from that of other selected HMs. Since the deposition forms of the HM salts on the MCFA surface are determined by the bonding types between adsorbates and adsorbents, the Cu^{2+} was regarded to have more stabilized chelating ring structures, and its adsorption behavior was regarded to tend more monolayer adsorption. Isotherm models discriminate the adsorption capacity for the highly active sites of the adsorbent with a large surface area and higher porosity (Zhou et al., 2018).

3.2.3 Adsorption kinetic models

Figure 11 and Table 4 show the effect of the contact time of MCFA on Mn^{2+}, Cu^{2+}, Ni^{2+}, and Pb^{2+}. The adsorption process was very fast at the initial contact time and slowed down at the final stage (after 60 min), ultimately reaching equilibrium. The study stated that at the beginning of the adsorption, there were more active sites and larger surface area of the adsorbent, but with passing time of adsorption, the reaction sites and surface area of the adsorbent decreased, and ultimately adsorption was decreased (Anuar, 2020). The fitting curves showed that the values of the correlation coefficient (R^2) for Mn^{2+}, Cu^{2+}, Ni^{2+}, and Pb^{2+} metal ions were higher (R^2 > 0.99) by pseudo-second-order than pseudo-first-order (R^2 < 0.97). The pseudo-second-order model indicated that the higher surface area of MCFA adsorbed the HM ions through physical adsorption.

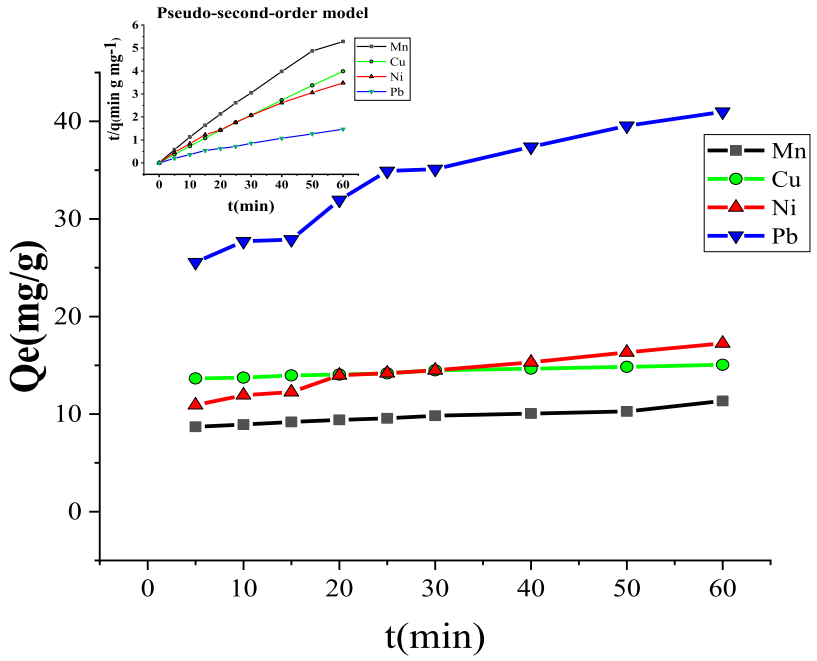

FIGURE 11
Kinetic curves of MCFA adsorption of four HMs.

TABLE 4 Kinetic parameter models for four HMs by the MCFA adsorbent.

Model	Parameter	Mn^{2+}	Cu^{2+}	Ni^{2+}	Pb^{2+}
Pseudo-first-order	K_1 10^{-2} (L/min)	0.27	0.29	0.24	0.13
	q_e (mg/g)	376.53	240.54	232.29	224.80
	R^2	0.9702	0.9675	0.9287	0.9402
Pseudo-second-order	K_2 10^{-3} (g/mg/min)	0.27	0.37	1.17	3.31
	q_e (mg/g)	74.63	71.94	56.50	44.64
	R^2	0.9919	0.9908	0.9945	0.9924

Table 4 shows the adsorption mechanism of the kinetic model for selected HMs. The kinetic parameters indicated that the values of the correlation coefficient (R^2) of both kinetic models (R^2 < 0.97 and R^2 > 0.99) for pseudo-first-order and pseudo-second-order, respectively, was close to each other. The results showed the MCFA adsorptive behaviors for the ions were driven by both physical and chemical forces. The adsorption capacity was recorded to be higher (376.53, 240.54, 232.29, and 224.80 mg/g) for Mn^{2+}, Cu^{2+}, Ni^{2+}, and Pb^{2+}, respectively, by pseudo-first-order. The study indicated that the electron transfer reactions (ion exchange and chelation action) played a significant role in the adsorption process, which was in accordance with the results of the adsorption isotherm (Jang et al., 2018).

3.2.4 Effect of anions on modified flocculants particles of coal fly ash adsorption of heavy metals

The wastewater is a mixture of complex pollutants, which affect the removal of selected pollutants from wastewater. Figure 12 shows the effect of three anions Cl^-, SO_4^{2-}, and NO_3^- on the adsorption of MCFA for the removal of HMs. The experimental results showed that there is a smaller inhibitory effect on all three anions (Cl^-, SO_4^{2-}, and NO_3^-) for the removal of Mn^{2+}. Similarly, $Cl^-$and SO_4^{2-} showed an effect for the removal of Cu^{2+} and Ni^{2+}. The maximum removal efficiency by SO_4^{2-} was recorded at 92.91% and 92.23% for Cu^{2+} and Ni^{2+}, respectively, but overall maximum removal efficiency was recorded at 98.46% by the effect of NO_3^- ion for Pb^{2+}. There might be two reasons

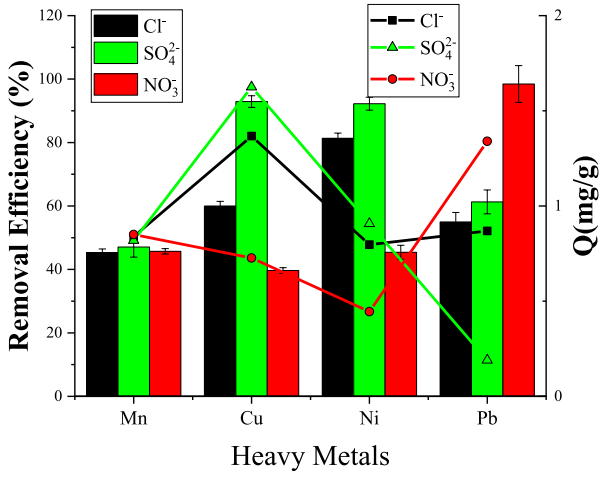

FIGURE 12
Effect of anions on the surface of MCFA for the removal of four HMs.

for the maximum removal efficiency of Pb^{2+}, one is the physical structure of the adsorbent including pore diameter and volume and the other is the hydrated ionic radii of the metals. The ionic radii of Pb^{2+} are smaller (0.401 nm) than those of Cu^{2+} and Ni^{2+} (0.419 and 0.404 nm, respectively) (Wang et al., 2019). The repulsion between Pb^{2+} and dissociated oxygen-containing groups was lower; therefore, Pb^{2+} ions have a higher ion-exchange capacity on the MCFA surface, and the anions affect the surface of the adsorbent for the adsorption process (Rivera-Utrilla et al., 2013). Since the sulfate radical is a divalent anion, which has stronger attractions to metal cations, so Pb^{2+} with the smallest hydrated ionic radius is regarded to have greater interaction with SO_4^{2-} anions, thus reducing the combining capacity to MCFA, but Cu^{2+} with smaller hydrated ionic radius can increase its adsorption capacity to MCFA because it has a bigger hydrated ionic radius, and thus has a lower interaction with SO_4^{2-} anions in aqueous solution. The difference in adsorption mechanisms decides the competitive adsorption of different ions on MCFA.

4 Conclusion

In order to promote the utilization and modification of coal fly ash, the flocculant particles of MCFA were prepared for the adsorption of selected HMs (Mn^{2+}, Cu^{2+}, Ni^{2+}, and Pb^{2+}). The CFA was modified by a multi-step acid–base modification reaction and flocculant porous materials of MCFA were obtained. The characterization results of SEM, EDX, BET, FT-IR, XPS, and XRD included that the MCFA has significantly increased surface area and oxygen-containing group (OCG) content.

The results indicated that the newly synthesized MCFA porous material has been changed from waste coal fly ash to active adsorbent material and has higher adsorbent capacity for HMs (Mn^{2+}, Cu^{2+}, Ni^{2+}, and Pb^{2+}). The batch sorption experiments found that the maximum removal efficiency (99.91% and 95.88%) was recorded for the removal of Pb^{2+} and Cu^{2+}. The results of the isotherm and kinetic models indicated that the adsorption might be monolayer adsorption, physical, and chemical, but it is concluded that the physical adsorption results were more promising due to the structural modification of the MCFA. The increased superficial area and OCG content are considered to be the intrinsic factor for the improved HM removal of MCFA.

Data availability statement

The data analyzed in this study are subject to the following licenses/restrictions: All the data materials are provided in the manuscript. Requests to access these datasets should be directed to Zawar Hussain, hussain.zawar1292@hotmail.com.

Author contributions

ZH: conceptualization, writing—original draft preparation, and methodology. HZ: reviewing and editing. NC: reviewing, editing, and funding. WH: supervision and funding.

Funding

This research is supported by the National Key Research and Development Program of China (2019YFC0408400).

Conflict of interest

The authors declare that the research was conducted in the absence of any commercial or financial relationships that could be construed as a potential conflict of interest.

Publisher's note

References

Anuar, S. A., Wan Isahak, W. N. R., and Masdar, M. S. (2020). Carbon nanoflake hybrid for biohydrogen CO 2 capture : Breakthrough adsorption test. *Int. J. Energy Res.* 44, 3148–3159. doi:10.1002/er.5169

Athman, S., Sdiri, A., and Boufatit, M. (2020). Spectroscopic and mineralogical characterization of bentonite clay (ghardaïa, Algeria) for heavy metals removal in aqueous solutions. *Int. J. Environ. Res.* 14 (1), 1–14. doi:10.1007/s41742-019-00232-6

Ayari, F., Srasra, E., and Trabelsi-Ayadi, M. (2008). Low-cost adsorbents for a dye uptake from contaminated water modeling of adsorption isotherms: The Langmuir, Freundlich and Elovich models. *Surf. Engin. Appl. Electrochem.* 44 (6), 489–498. doi:10.3103/S1068375508060112

Bai, S., Chu, M., Zhou, L., Chang, Z., Zhang, C., and Liu, B. (2019). Removal of heavy metals from aqueous solutions by X-type zeolite prepared from combination of oil shale ash and coal fly ash. *Energy Sources, Part A Recovery, Util. Environ. Eff.* 00 (00), 5113–5123. doi:10.1080/15567036.2019.1661549

Chen, H., Wang, X., Li, J., and Wang, X. (2015). Cotton derived carbonaceous aerogels for the efficient removal of organic pollutants and heavy metal ions. *J. Mat. Chem. A Mat.* 3 (11), 6073–6081. doi:10.1039/c5ta00299k

Cheng, Z. L., Li, Y. xiang, and Liu, Z. (2018). Study on adsorption of rhodamine B onto Beta zeolites by tuning SiO2/Al2O3 ratio. *Ecotoxicol. Environ. Saf.* 148 (), 585–592. doi:10.1016/j.ecoenv.2017.11.005

Clemens, S., and Ma, J. F. (2016). Toxic heavy metal and metalloid accumulation in crop plants and foods. *Annu. Rev. Plant Biol.* 67 (), 489–512. doi:10.1146/annurev-arplant-043015-112301

He, S., Li, Y., Weng, L., Wang, J., He, J., Liu, Y., et al. (2018). Competitive adsorption of Cd2+, Pb2+ and Ni2+ onto Fe3+-modified argillaceous limestone: Influence of pH, ionic strength and natural organic matters. *Sci. Total Environ.* 637, 69–78. –638. doi:10.1016/j.scitotenv.2018.04.300

Hong, M., Yu, L., Wang, Y., Zhang, J., Chen, Z., Dong, L., et al. (2019). *Chem. Eng. J.*, 359. Elsevier B.V. doi:10.1016/j.cej.2018.11.087 Heavy metal adsorption with zeolites: The role of hierarchical pore architecture

Hussain, Z., Chang, N., Sun, J., Xiang, S., Ayaz, T., Zhang, H., et al. (2022). Modification of coal fly ash and its use as low-cost adsorbent for the removal of directive, acid and reactive dyes. *J. Hazard. Mater.* 422 (2021), 126778. doi:10.1016/j.jhazmat.2021.126778

Iqbal, M., Saeed, A., and Iqbal, S. (2009). FTIR spectrophotometry , kinetics and adsorption isotherms modeling , ion exchange , and EDX analysis for understanding the mechanism of Cd 2 + and Pb 2 + removal by mango peel waste. *J. Hazard. Mat.* 164, 161–171. doi:10.1016/j.jhazmat.2008.07.141

Jang, H. M., Yoo, S., Choi, Y. K., Park, S., and Kan, E. (2018). Adsorption isotherm, kinetic modeling and mechanism of tetracycline on Pinus taeda-derived activated biochar. *Bioresour. Technol.* 259 (), 24–31. doi:10.1016/j.biortech.2018.03.013

Juang, L. C., Wang, C. C., and Lee, C. K. (2006). Adsorption of basic dyes onto MCM-41. *Chemosphere* 64 (11), 1920–1928. doi:10.1016/j.chemosphere.2006.01.024

Lavall, R. L., Assis, O. B. G., and Campana-Filho, S. P. (2007). β-Chitin from the pens of Loligo sp.: Extraction and characterization. *Bioresour. Technol.* 98 (13), 2465–2472. doi:10.1016/j.biortech.2006.09.002

Lee, Y. R., Soe, J. T., Zhang, S., Ahn, J. W., Park, M. B., and Ahn, W. S. (2017). Synthesis of nanoporous materials via recycling coal fly ash and other solid wastes: A mini review. *Chem. Eng. J.* 317, 821–843. doi:10.1016/j.cej.2017.02.124

Maleki, A., Hajizadeh, Z., Sharifi, V., and Emdadi, Z. (2019). A green, porous and eco-friendly magnetic geopolymer adsorbent for heavy metals removal from aqueous solutions. *J. Clean. Prod.* 215, 1233–1245. doi:10.1016/j.jclepro.2019.01.084

Mushtaq, F., Zahid, M., Mansha, A., Bhatti, I. A., Mustafa, G., Nasir, S., et al. (2020). MnFe2O4/coal fly ash nanocomposite: A novel sunlight-active magnetic photocatalyst for dye degradation. *Int. J. Environ. Sci. Technol. (Tehran).* 17 (10), 4233–4248. doi:10.1007/s13762-020-02777-y

Nguyen, T. C., Tran, T. D. M., Dao, V. B., Vu, Q. T., Nguyen, T. D., and Thai, H. (2020). Using modified fly ash for removal of heavy metal ions from aqueous solution. *J. Chem.* 2020, 1–11. doi:10.1155/2020/8428473

Niu, M., Li, G., Cao, L., Wang, X., and Wang, W. (2020). Preparation of sulphate aluminate cement amended bentonite and its use in heavy metal adsorption. *J. Clean. Prod.* 256, 120700. doi:10.1016/j.jclepro.2020.120700

Qiu, R., Cheng, F., and Huang, H. (2018). Removal of Cd2+ from aqueous solution using hydrothermally modified circulating fluidized bed fly ash resulting from coal gangue power plant. *J. Clean. Prod.* 172, 1918–1927. doi:10.1016/j.jclepro.2017.11.236

Rivera-Utrilla, J., Gómez-Pacheco, C. V., Sánchez-Polo, M., López-Peñalver, J. J., and Ocampo-Pérez, R. (2013). Tetracycline removal from water by adsorption/bioadsorption on activated carbons and sludge-derived adsorbents. *J. Environ. Manag.* 131, 16–24. doi:10.1016/j.jenvman.2013.09.024

Salehin, S., Aburizaiza, A. S., and Barakat, M. A. (2016). Activated carbon from residual oil fly ash for heavy metals removal from aqueous solution. *Desalination Water Treat.* 57 (1), 1–10. doi:10.1080/19443994.2015.1006824

Shah, B., Mistry, C., and Shah, A. (2013). Seizure modeling of Pb(II) and Cd(II) from aqueous solution by chemically modified sugarcane bagasse fly ash: Isotherms, kinetics, and column study. *Environ. Sci. Pollut. Res.* 20 (4), 2193–2209. doi:10.1007/s11356-012-1029-3

Song, M., Wei, Y., Cai, S., Yu, L., Zhong, Z., and Jin, B. (2018). Study on adsorption properties and mechanism of Pb2 + with different carbon based adsorbents. *Sci. Total Environ.* 618, 1416–1422. doi:10.1016/j.scitotenv.2017.09.268

Tang, J., Su, M., Wu, Q., Wei, L., Wang, N., Xiao, E., et al. (2019). Highly efficient recovery and clean-up of four heavy metals from MSWI fly ash by integrating leaching, selective extraction and adsorption. *J. Clean. Prod.* 234, 139–149. doi:10.1016/j.jclepro.2019.06.198

Visa, M., and Chelaru, A. M. (2014). Hydrothermally modified fly ash for heavy metals and dyes removal in advanced wastewater treatment. *Appl. Surf. Sci.* 303, 14–22. doi:10.1016/j.apsusc.2014.02.025

Wang, Li, Wang, Y., Ma, F., Tankpa, V., Bai, S., Guo, X., et al. (2019). Mechanisms and reutilization of modified biochar used for removal of heavy metals from wastewater: A review. *Sci. Total Environ.* 668, 1298–1309. doi:10.1016/j.scitotenv.2019.03.011

Wang, Lu, Huang, X., Zhang, J., Wu, F., Liu, F., Zhao, H., et al. (2021). Stabilization of lead in waste water and farmland soil using modified coal fly ash. *J. Clean. Prod.* 314 (), 127957. doi:10.1016/j.jclepro.2021.127957

Yang, S., Zhao, D., Zhang, H., Lu, S., Chen, L., and Yu, X. (2010). Impact of environmental conditions on the sorption behavior of Pb(II) in Na-bentonite suspensions. *J. Hazard. Mater.* 183 (1–3), 632–640. doi:10.1016/j.jhazmat.2010.07.072

Yuan, Y., An, Z., Zhang, R., Wei, X., and Lai, B. (2021). Efficiencies and mechanisms of heavy metals adsorption on waste leather-derived high-nitrogen activated carbon. *J. Clean. Prod.* 293, 126215. doi:10.1016/j.jclepro.2021.126215

Zhang, Y., Wang, P., Hussain, Z., Zhang, H., Wang, H., Chang, N., et al. (2022). Modification and characterization of hydrogel beads and its used as environmentally friendly adsorbent for the removal of reactive dyes. *J. Clean. Prod.* 342 (2021), 130789. doi:10.1016/j.jclepro.2022.130789

Zhou, Y., Hu, Y., Huang, W., Cheng, G., Cui, C., and Lu, J. (2018). A novel amphoteric B-cyclodextrin-based adsorbent for simultaneous removal of cationic/anionic dyes and bisphenol A. *Chem. Eng. J.* 341, 47–57. doi:10.1016/j.cej.2018.01.155

Zhu, Y., Fan, W., Zhou, T., and Li, X. (2019). Removal of chelated heavy metals from aqueous solution: A review of current methods and mechanisms. *Sci. Total Environ.* 678 (37), 253–266. doi:10.1016/j.scitotenv.2019.04.416